Available online at www.sciencedirect.com

SciVerse ScienceDirect

Physics Procedia 46 (2013) 118 – 126

Physics Procedia

Nineteenth European Conference on Chemical Vapor Deposition, (EUROCVD 19)

Multifunctional manganese single source precursor for the selective deposition of MnF_2 or Mn_3O_4

Maria R. Catalano, and Graziella Malandrino*

Dipartimento di Scienze Chimiche, Università di Catania, ISTM-CNR, and INSTM UdR Catania, V.le Andrea Doria 6, 95125 Catania, Italy.

Abstract

A novel Mn(II) precursor, the $Mn(hfa)_2$●tmeda, was successfully applied to the deposition of manganese containing nanostructures in Metal Organic Chemical Vapor Deposition (MOCVD) processes at atmospheric and reduced pressure. Experimental data evidenced that different phases were obtained, selectively and reproducibly, on varying the operating pressure. Manganese difluoride (MnF_2) nanorod assemblies were obtained under atmospheric pressure, while hausmannite (Mn_3O_4) nanostructured films were obtained under reduced pressure. X-ray diffraction patterns in grazing incidence mode and energy dispersive X-ray analyses confirmed the phase nature and composition of the manganese containing nanostructures. Field-emission scanning electron microscopy images evidenced the nanostructure morphology of both the MnF_2 and Mn_3O_4 phases.

Keywords: Manganese (II) precursor; nanorod assembly; manganese difluoride; hausmannite film.

* Corresponding author. Graziella Malandrino Tel.: +39-095-7385055; fax: +39-095-580138.
E-mail address: gmalandrino@dipchi.unict.it.

doi:10.1016/j.phpro.2013.07.053

1. Introduction

Recently, a renewed interest has grown regarding possible routes to high quality thin films of various manganese-containing materials. Manganese is an important component in several classes of materials such as solid electrolytes in Li based batteries [1], magnetoresistive oxide perovskites such as $La_{1-x}A_xMnO_{3-\delta}$ [2,3] and $Pr_{1-x}Ca_xMnO_3$ [4,5], multiferroic Bi-Mn-O phases [6] and simple manganese oxides such as Mn_3O_4 [7,8], which has been used as an active catalyst. The most used manganese precursor is the $Mn(tmhd)_3$ (Htmhd = 2,2,6,6-tetramethyl-3,5-heptanedione) [9]. Nevertheless, for some kind of applications, Mn(II) precursors are needed. For e.g. Mn(II) is widely used as a magnetic dopant in III-V and II-VI semiconductors to prepare diluted magnetic semiconductor systems [10-12]. Very few examples are known in the literature of Mn(II) precursor, essentially based on cyclopentadienyl ligand, but, even though +2 is the most stable oxidation state for manganese, the chemistry of manganese(II) β-diketonates has not been explored as extensively as the chemistry of manganese(III) β-diketonates. This is due to an easy decomposition of Mn(II) complexes with unfluorinated β-diketonates under formation of the corresponding manganese(III) complex, and to the coordination of water molecules when the coordination sphere is not saturated. In addition, a fluorinated β-diketonate Mn(II) complex may be envisaged as a Mn-F single source for the fabrication of MnF_2 thin films, that are interesting in device fabrication for their antiferromagnetic properties [13, 14], and of fluoroperovskite nanostructures such as $NaMnF_3$ e $KMnF_3$. These fluoroperovskite phases have attracted extensive attention as a result of their size-dependent properties, such as magnetic, piezoelectric and, when doped with rare-earth ions, photoluminescent behavior [15,16].

In the present work, we report on the transport properties of a new manganese(II) precursor, the $Mn(hfa)_2$•tmeda [(H-hfa = 1,1,1,5,5,5-hexafluoro-2,4-pentandione, tmeda = N,N,N',N'-tetramethylethylendiamine)] and on its functional validation through applications in MOCVD processes. In particular, the complex shows a remarkable volatility even at atmospheric pressure which allowed its use not only under vacuum but also under very mild MOCVD conditions, i.e. in atmospheric pressure MOCVD processes. The study reports on the relationship between deposition parameters and deposited phases. It is interesting to comment on the effect of pressure since depositions at atmospheric pressure give rise, reproducibly and selectively, to MnF_2 nanostructures [17], while depositions under reduced pressure produce highly structured Mn_3O_4 films [18].

2. Experimental

Mn containing films were prepared in a horizontal, home-made, hot wall MOCVD reactor (diameter = 25 mm, length = 800 mm) from the $Mn(hfa)_2$•tmeda, precursor contained in a resistively heated alumina boat under atmospheric or reduced pressure (3 torr). A scheme of the hot-wall reactor used for this study is reported in Fig. 1.

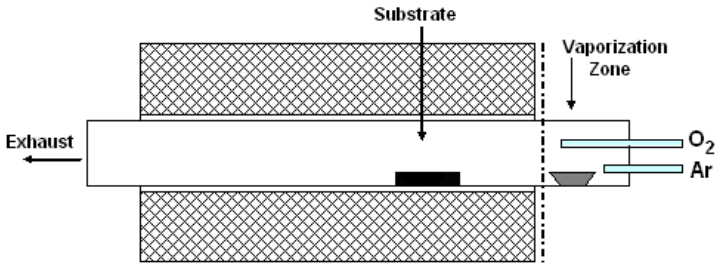

Fig. 1. Reactor scheme.

Si (100) substrates were used for the depositions. In this study, the precursor evaporation temperature was kept at 80°C (P = 3 torr) or 130°C (atmospheric pressure), while the reactor temperature was varied in the range 450-650°C. Ar (150 sccm) and O_2 (150 sccm) flows were used as carrier and reaction gases, respectively. The mass flows were controlled with 1160 MKS flowmeter using an MKS 147 electronic control unit. Depositions were carried out for 60 minutes.

θ-2θ X-ray diffraction (XRD) patterns were recorded in grazing incidence mode (0.8°) on a Bruker–AXS D5005 θ-θ X-ray diffractometer, using a Göebel mirror to parallel Cu-Kα radiation operating at 40 KV and 30 mA. The surface morphologies were examined by field emission scanning electron microscopy (FE-SEM) using a ZEISS VP 55 microscope. Energy dispersive X-ray analyses (EDX) spectra were obtained using a "windowless" Oxford Inca Energy detector.

3. Results and discussion

3.1 Precursor synthesis and thermal properties

The single-source Mn/F or Mn/O precursor has been synthesized through a one step reaction, from manganese(II) acetate tetrahydrate, hexafluoroacetylacetone and N,N,N',N'- tetramethylethylenediamine in dichlorometane (Eq. (1)) [18].

$$Mn(CH_3COO)_2 \bullet 4H_2O + 2Hhfa + tmeda \rightarrow Mn(hfa)_2 \bullet tmeda + 2\ CH_3COOH + 4H_2O \qquad (1)$$

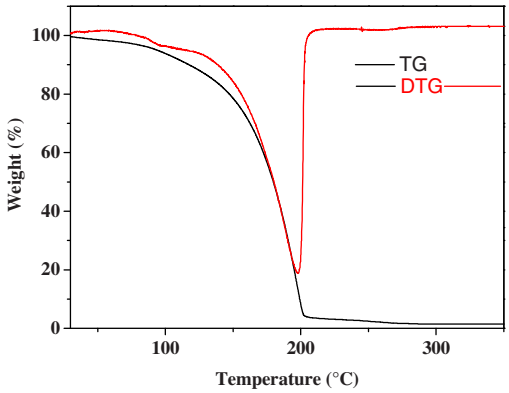

Fig. 2. TG profile and derivative curve (DTG) of the $Mn(hfa)_2$•tmeda adduct in the 25-350°C temperature range.

The TG profile (Fig. 2) recorded at atmospheric pressure in purified nitrogen flow indicates that the $Mn(hfa)_2$●tmeda adduct is thermally stable and evaporates quantitatively in the 100-230 °C temperature range, with a 1.5 % residue at 300 °C. The melting point of the product is 71-74 °C, thus the precursor is a liquid under both vaporization temperatures. The $Mn(hfa)_2$•tmeda precursor has been validated through its successful application to the fabrication of manganese containing films.

A crucial parameter in these depositions is the processing pressure. Fig. 3 represents a scheme of the results obtained under atmospheric pressure and reduced pressure. In fact, experiments have shown that the use of the $Mn(hfa)_2$●tmeda precursor yields, reproducibly and selectively, MnF_2 nanostructures under atmospheric pressure and Mn_3O_4 nanostructured films under reduced pressure.

The other processing parameters, such as deposition temperatures, do not play a significant role in the phase formation. Mixed phases were never observed. Processing conditions are schematized in Table 1.

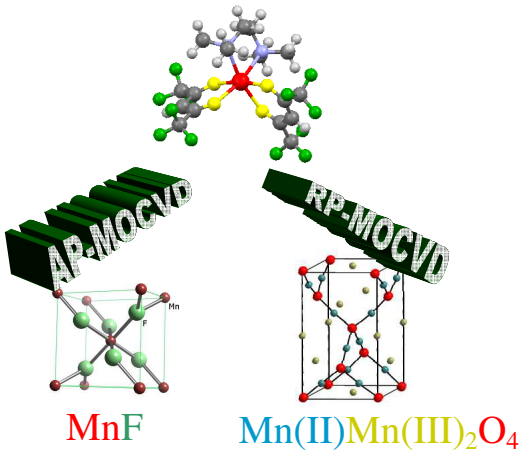

Fig. 3. Scheme of products obtained from the MOCVD of the $Mn(hfa)_2$●tmeda precursor at atmospheric (AP) and reduced pressure (RP).

Table 1. Processing parameters used for the deposition of the Mn containing films.

T_{vap} (°C)	T_{dep} (°C)	Carrier gas (Ar) (sccm)	Reaction gas (O_2) (sccm)	Pressure (torr)	Film composition
80	500-650	150	150	3	Mn-O
130	450-600	150	150	760	Mn-F

3.2 Deposition of MnF_2 nanostructures

The XRD pattern of the nanostructures deposited at 600°C under atmospheric pressure (Fig. 4a) shows the formation of a polycrystalline MnF_2 phase since all the peaks can be associated with reflections of the polycrystalline powder [ICDD N°. 24-0727]. The energy dispersive X-ray (EDX) spectrum (Fig. 4b) confirmed the chemical composition of the nanostructures, composed of manganese and fluorine only. The manganese K_α and K_β peaks are observed at 5.887 and 6.496 keV, while the L lines are found at 0.637 keV.

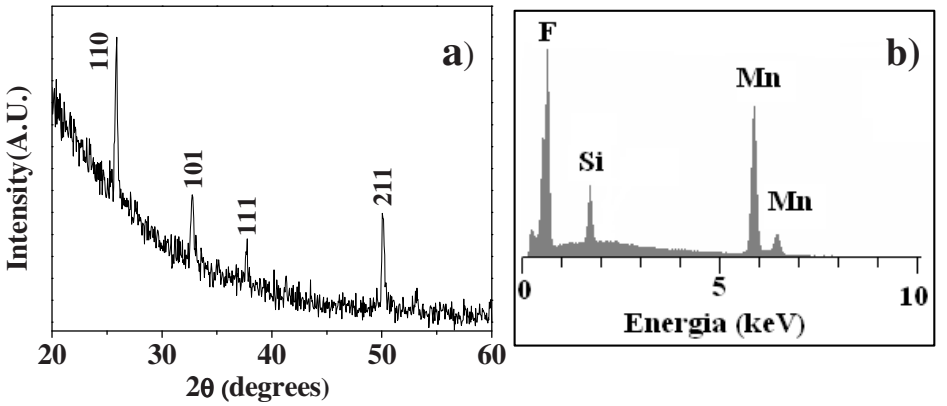

Fig. 4. (a) XRD pattern and (b) EDX spectrum of the MnF_2 nanostructures.

In addition, the windowless EDX detector allowed to exclude the presence of O in the nanorods, since the O K_α peak at 0.520 keV is not found. Characterization showed similar results for films deposited in the 450-600°C temperature range

A Si substrate 0.8 x 4 cm^2 has been used to observe variation in morphology of the deposited system. In Fig. 5 the morphology of the MnF_2 phase deposited on Si at 600 °C for 1 h is reported. The zero in the ruler indicates the initial part of the substrate, the nearest to the precursor inlet. In the initial part (0-1.5 cm), a film layer with cubic or leaf-like crystallites is formed. Around 2 cm, the pompon-like nanostructure is observed, while toward the end of the substrate a cauliflower-like morphology is found.

A rationalization of this behaviour is not an easy task, but it can be excluded that the different morphology may depend on temperature.

The substrate (4 cm length) is small to have a significant different temperature along its length, so the various morphologies have to be associated with the amount of precursor over the substrate. Note in this context, that depositions are carried out under atmospheric pressure and therefore some unusual behaviour of the flow could be possible.

Thus it is likely, that the surface morphology of the as-deposited structures is determined by the complex interplay between mass transport and surface kinetics of the system. In the present case, the supersaturation degree (μ) of the precursor and the growth rate seems to play a crucial role in determining the morphology of MnF_2 nanorods.

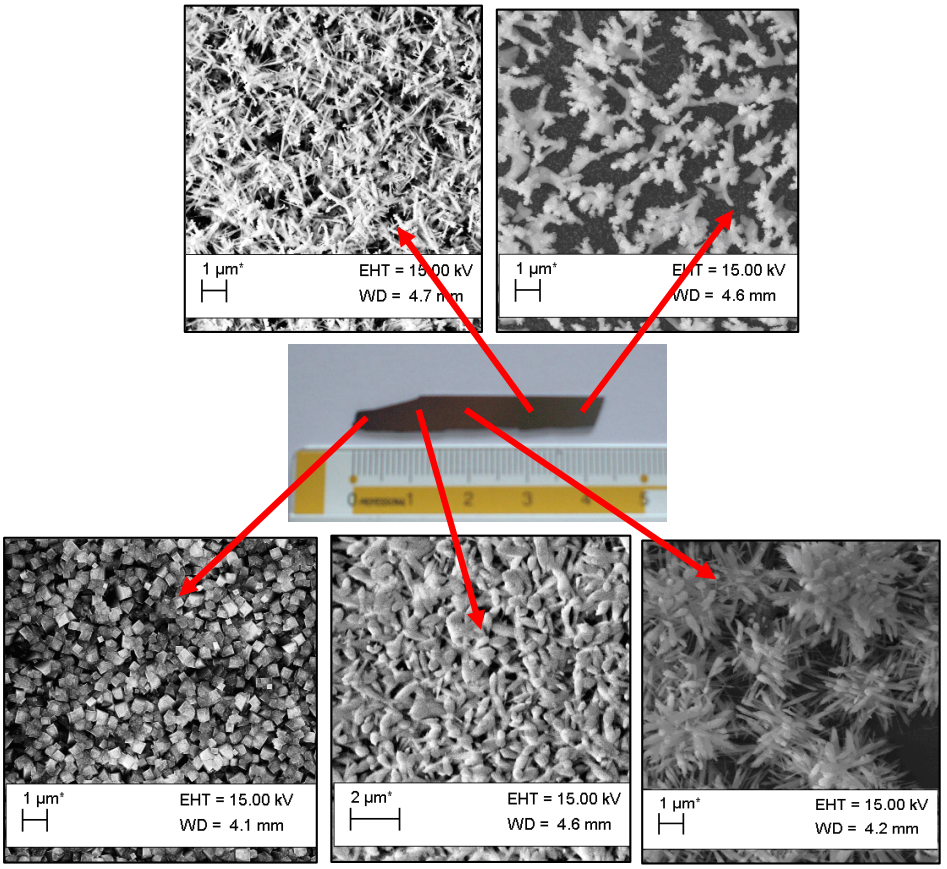

Fig. 5. Variation of morphology for the MnF_2 phase deposited on Si at 600°C for 1h.

3.3 Deposition of Mn_3O_4 nanostructured films

XRD patterns have been recorded in grazing incidence mode. Films deposited at 550°C under reduced pressure (Fig. 6a) exhibit several peaks, the most intense at 2θ = 28.9°, 30.8°, 32.6°, 36.0°, 44.3° and 58.4° that may be associated with the 112, 200, 103, 211, 220 and 321 reflections, respectively, of the spinel tetragonal Mn_3O_4 phase (a = 5.762 Å and c = 9.469 Å) [ICDD n. 24-0734]. The relative intensities do not match exactly those reported in the ICDD database, nevertheless no preferential orientation is evident. The EDX spectrum, reported in Fig. 6b, shows the presence of the Mn K_α and K_β peaks at 5.895 and 6.490 keV, respectively, and the O Kα peak at 0.560 KeV. The peak at 1.730 KeV is due to Si Kα peak of the Si substrate. Finally, the surface morphology of the Mn_3O_4 film has been investigated by scanning electron microscopy. The sample (Fig. 7) presents a very uniform nanostructured morphology with grains less than 100 nm in diameters. Outgrowths with a dentelled leaf-like structure about 600nm wide and 60 nm thick come out from the surface structure. Similar results have been found in the investigated temperature range of 500-650°C.
Thus under reduced pressure, the $Mn(hfa)_2$•tmeda represents a single source of Mn and oxygen.

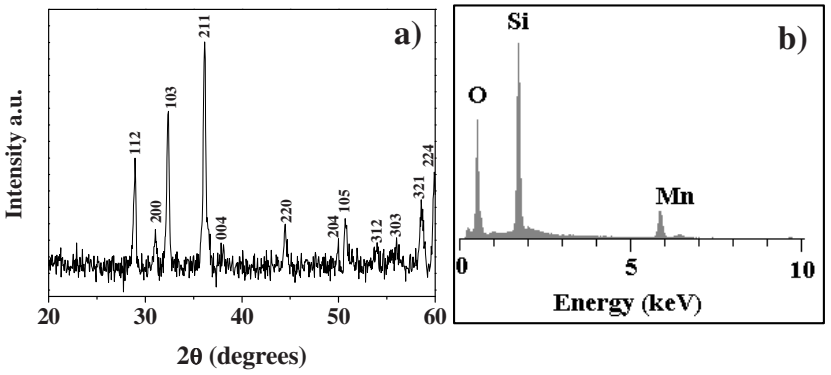

Fig. 6. (a) XRD pattern and (b) EDX spectrum of the Mn_3O_4 nanostructured films.

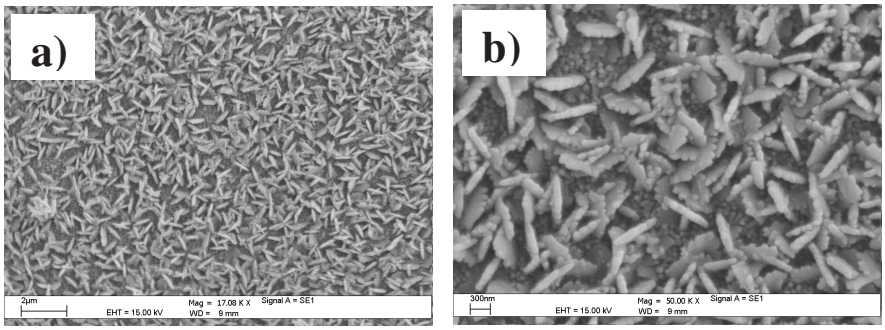

Fig. 7. SEM images at (a) low and (b) high magnification of the Mn_3O_4 nanostructured films.

Finally, it is interesting to comment on the different products obtained for depositions carried out from the $Mn(hfa)_2$•tmeda under vacuum or atmospheric pressure. This different behaviour may be explained considering that typically this kind of precursor produces F source during the decomposition, thus when the deposition is carried out at atmospheric pressure the F source has the time to react with the Mn^{2+} ion yielding

the MnF_2 nanostructures. At low pressure the F local concentration is too low to give rise to the manganese difluoride formation, and instead the spinel Mn_3O_4 phase is formed. These findings are in accordance with data reporting that manganese oxides react with F_2 diluted with N_2 already at 100°C to produce MnF_3 and minor amounts of MnF_2 [19].

5. Conclusions

Present investigations clearly indicate that the $Mn(hfa)_2$●tmeda represents a suited precursor for the deposition of manganese-containing films. The TG measurements show a remarkable volatility with a low residue even at atmospheric pressure, characteristics that allowed its use not only under reduced pressure depositions but also under very mild MOCVD conditions, i.e. in AP-MOCVD processes. These properties together with its low melting point make this precursor usable in the liquid phase without decomposition, providing constant evaporation rates even for very long deposition times, and thus very appealing in MOCVD processes.

Finally, this precursor represents a multifunctional source that depending on the operating conditions can behave as a clean single source of manganese and fluorine or as a source of manganese and oxygen. In particular, it can be applied to a bottom-up approach for the fabrication of MnF_2 nanorod assembly, in a pompon-like fashion, or of nanostructured Mn_3O_4 films.

Acknowledgements

The authors thank the MIUR for the financial support within the PRIN 2009 N. 20097X44S7_002.

References

[1] J. Proell, R. Kohler, A. Mangang, S. Ulrich, C. Ziebert, W. Pfleging, "3D structures in battery materials", *J. Laser Micro/Nanoeng.* 2012. *7,* p. 97.

[2] C. Dubourdieu, M. Rosina, H. Roussel, F. Weiss, J. P. Senateur, J. L. Hodeau, Pulsed liquid-injection metalorganic chemical vapor deposition of ($La_{0.7}Sr_{0.3}MnO_3/SrTiO_3$) superlattices, Appl. Phys. Lett. 2001, 79, p. 1246.

[3] R. G. Toro, D. M.R. Fiorito, M. E. Fragalà, A. Barbucci, M. P. Carpanese, G. Malandrino, A novel MOCVD strategy for the fabrication of cathode in a solid oxide fuel cell: Synthesis of $La_{0.8}Sr_{0.2}MnO_3$ films on YSZ electrolyte pellets, Mater. Chem. Phys. 2010, 124**,** p. 1015.

[4] T. Nakamura, R. Tai, K. Tachibana, Metalorganic chemical vapor deposition of magnetoresistive manganite films exhibiting electric-pulse-induced resistance change effect, J. Appl. Phys. 2006, 99, 08Q302/1.

[5] S. Y. Zhou, Y. Zhu, M. C. Langner, Y.-D. Chuang, P. Yu, W. L. Yang, , A. G. Cruz Gonzalez, N. Tahir, M. Rini, Y.-H. Chu, R. Ramesh, D.-H. Lee, Y. Tomioka, Y. Tokura, Z. Hussain, R. W. Schoenlein, Ferromagnetic enhancement of CE-type spin ordering in (Pr, Ca)MnO_3, Phys. Rev. Lett. 2011, 106, 186404/1.

[6] H. Jeen, G. Singh-Bhalla, P. R. Mickel, K. Voigt, C. Morien, S. Tongay, A. F. Hebard, A. Biswas, Growth and characterization of multiferroic $BiMnO_3$ thin films, J. Appl. Phys. 2011, 109(7), 074104/1**.**

[7] O. Y. Gorbenko, I. E. Graboy, V. A. Amelichev, A. A.; Bosak, A. R. Kaul, B. Guttler, V. L. Svetchnikov, H. W. Zandbergen, The structure and properties of Mn_3O_4 thin films grown by MOCVD, Solid State Comm. 2002, 124, 15.

[8] L. W. Guo, D. L. Peng, H. Makino, K. Inaba, H. J. Ko,K. Sumiyama, T. Yao, Structural and magnetic properties of Mn3O4 films grown on MgO(0 0 1) substrates by plasma-assisted MBE, J. Magnetism Magnetic Mater. 2000, 213, 321.

[9] T. Nakamura, R. Tai, T. Nishimura, K. Tachibana, Composition control of manganite perovskites in metalorganic chemical vapor deposition with in situ spectroscopic monitoring, J. Appl. Phys. 2005, 97, 10H712/1.

[10] M. H. Kane , A. Asghar , A. M. Payne , C. R. Vestal , Z. J. Zhang , M. Strassburg , J. Senawirante, N. Dietz , C. J. Summers, I. T. Ferguson, Magnetic and optical properties of $Ga_{1-x}MnxN$ grown by metalorganic chemical vapour deposition, Semicond. Sci. Technol. 2005, *20***,** L5.

[11] L. Zhang, J.-Q. Wang, J. Li, S. Zhang, Z. Jiang, J. Zhou, J. Cheng, T. Hu, W. Yan, X. Wei, Xiangjun, Regulation of Magnetic Behavior and Electronic Configuration in Mn-Doped ZnO Nanorods through Surface Modifications, Chem. Mater. 2012, 24, 1676.

[12] X. X. Lin, Y. F. Zhu, W. Z. Shen, Synthesis and Optical and Magnetic Properties of Diluted Magnetic Semiconductor $Zn_{1-x}Mn_xO$

Hollow Spherical Structures, J. Phys. Chem. C 2009, 113, 1812.
[13] Y. Zhao, Yan, S.-F. Fu, H. Li, X.-Z. Wang, Bistable transmission of antiferromagnetic Fabry-Perot resonator, J. Appl.Phys. 2011, 110 023512/1.
[14] V. Veerakumar, R. E. Camley, Magnetostatic bulk and surface spin-wave focusing in antiferromagnetic thin films, Phys. Rev. B 2010, 81, 174432.
[15] F. Zhang, Y. Mao, T.-J. Park, S. S. Wong, Green synthesis and property characterization of single-crystalline perovskite fluoride nanorods, Adv. Funct. Mater. 2008, 18, 103.
[16] Y.-P. Du, Y.-W. Zhang, Z.-G. Yan, L.-D. Sun, S. Gao, C.-H. Yan, Single-crystalline and near-monodispersed $NaMF_3$ (M = Mn, Co, Ni, Mg) and $LiMAlF_6$ (M = Ca, Sr) nanocrystals from co-thermolysis of multiple trifluoroacetates in solution, Chem.-An Asian J., 2007, 2, 965.
[17] G., Malandrino, R. G. Toro, M. R. Catalano, M. E. Fragalà, P. Rossi, P. Paoli, Pompon-Like MnF_2 Nanostructures from a Single-Source Precursor through Atmospheric Pressure Chemical Vapor Deposition, Eur. J. Inorg. Chem. 2012, 1021.
[18] Z. Lipani, M. R. Catalano, P. Rossi, P. Paoli, G. Malandrino, A Novel Manganese(II) MOCVD Precursor: Synthesis, Characterization, and Mass Transport Properties of $Mn(hfa)_2$•tmeda, Chem. Vap. Deposition, 2013, 19, 22.
[19] E. E. Aynsley, R. D. Peacock, P. L. Robinson, The reaction of fluorine with the oxides and oxy compounds of manganese and rhenium, J. Chem. Soc. 1950, 1622.